Eigenspace perturbations for uncertainty estimation of single-point turbulence closures

Gianluca Iaccarino, Aashwin Ananda Mishra,* and Saman Ghili
Center for Turbulence Research, Stanford University, Stanford, California 94305, USA
(Received 12 September 2016; published 27 February 2017)

Reynolds-averaged Navier-Stokes (RANS) models represent the workhorse for predicting turbulent flows in complex industrial applications. However, RANS closures introduce a significant degree of epistemic uncertainty in predictions due to the potential lack of validity of the assumptions utilized in model formulation. Estimating this uncertainty is a fundamental requirement for building confidence in such predictions. We outline a methodology to estimate this structural uncertainty, incorporating perturbations to the eigenvalues and the eigenvectors of the modeled Reynolds stress tensor. The mathematical foundations of this framework are derived and explicated. Thence, this framework is applied to a set of separated turbulent flows, while compared to numerical and experimental data and contrasted against the predictions of the eigenvalue-only perturbation methodology. It is exhibited that for separated flows, this framework is able to yield significant enhancement over the established eigenvalue perturbation methodology in explaining the discrepancy against experimental observations and high-fidelity simulations. Furthermore, uncertainty bounds of potential engineering utility can be estimated by performing five specific RANS simulations, reducing the computational expenditure on such an exercise.

DOI: 10.1103/PhysRevFluids.2.024605

I. INTRODUCTION

In spite of over a century of research, no analytical solutions for the equations governing turbulent flows are available. With the present state of computational resources, a purely numerical resolution of turbulent time and length scales encountered in engineering problems is not viable in industrial design practice. Consequently, almost all investigations have to resort to some degree of modeling. Turbulence models are constitutive relations attempting to relate quantities of interest to flow parameters using assumptions and simplifications derived from physical intuition and observations. Reynolds-averaged Navier-Stokes (RANS) -based models represent the pragmatic recourse for complex engineering flows, with a vast majority of simulations, in both academia and industry, resorting to this avenue. Despite their widespread use, RANS-based models suffer from an inherent structural inability to replicate fundamental turbulence processes and specific flow phenomena, as they introduce a high degree of epistemic uncertainty into the simulations arising due to the model form.

Uncertainty quantification for RANS-based closures attempts to assess the trustworthiness of model predictions of quantities of interest and is thus of considerable utility in establishing RANS models as tools for engineering applications. To address structural uncertainties, Singh and Duraisamy [1] and Parish and Duraisamy [2] utilize a data-driven approach wherein full-field data sets are utilized to infer and calibrate the functional form of model discrepancies. This is augmented by machine learning algorithms to reconstruct model corrections. Ling and Templeton [3] employ a data-driven approach along with a variety of machine learning algorithms to identify regions in the flow where high degrees of model-form uncertainty are extant. Recently, a physics-based nonparametric approach to estimate the model-form uncertainties has been developed by Emory *et al.* [4]. This framework approximates structural variability via sequential perturbations injected

*aashwin@stanford.edu

into the predicted Reynolds stress eigenvalues, eigenvectors, and the turbulent kinetic energy. This perturbation formulation of this approach has been applied to engineering problems with considerable success [5–8]. In a similar vein, Xiao *et al.* [9] and Wu *et al.* [10] have used a data-driven framework to inject perturbations into the Reynolds stress eigenvalues to ascertain model-form uncertainties.

However, a fundamental encumbrance in these studies arises due to the absence of a methodology to perturb the eigenvectors of the Reynolds stress tensor. The inconsistency in the eigenvector alignments between model predictions and experimental studies has been identified as a major source of discrepancy in the RANS modeling framework [9]. For instance, the eddy-viscosity hypothesis common to mixing-length models, as well as one-, two-, and three-equation closures such as the Spalart-Allmaras, k-ω, and v^2-f models, assumes that the Reynolds stress has the same eigenvectors as the mean rate of strain. This is known to be invalid in complex flows, for instance, those involving streamline curvature, flow separation, or rapid accelerations of the fluid [11–13]. Bereft of a complementary eigenvector perturbation framework, this perturbation methodology is deficient. Specifically, in flows with flow separation, its estimates of the uncertainty bounds are severely modest, affecting its utility as a tool to guide engineering decisions.

In this investigation, we outline a comprehensive framework for eigenspace perturbations to study the structural uncertainty in turbulence models. We focus on injecting uncertainty into the shape and the orientation of the Reynolds stress tensor to quantify the variability and biases introduced in the predictions. To ensure its engineering applicability, this framework attempts to assess the model uncertainty within the purview of single-point closures, without utilizing any additional data or modeling assumptions. In this vein, the perturbations of the Reynolds stress anisotropy are governed by sampling from the extreme states of the turbulence componentiality. Similarly, the perturbations to the Reynolds stress eigenvectors are guided by the maximal states of the production mechanism. Jointly, these provide for a schema wherein the approximate bounds due to model-form uncertainty can be estimated within five RANS simulations, reducing the computational overhead. After introducing the mathematical foundations underlying this framework in detail, as a proof of concept we apply this methodology to a set of separated turbulent flows while comparing to numerical and experimental data and contrasting against the predictions of the eigenvalue-only perturbation methodology. It must be stressed that the approach outlined herein introduces a perturbation strategy for the Reynolds stress eigenspace, but does not attempt to estimate the uncertainty due to the turbulent transport process. While turbulent kinetic energy perturbation strategies have been proposed [5,6], these have not been employed here as they require user-specified coefficients that might not be justified without additional supporting data. Additionally, the absence of a spatial discrepancy function further limits the comprehensive nature of the results. However, using these comparisons, we aim to exhibit that for separated flows, the eigenspace perturbation framework is able to yield considerable improvement over the eigenvalue perturbation methodology in recovering the discrepancy of the RANS predictions contrasted against experimental observations and data from high-fidelity simulations, without using any calibration data.

II. MATHEMATICAL DETAILS

The goal of Reynolds-averaged Navier-Stokes closures is to determine the Reynolds stress tensor in terms of mean flow quantities that are directly computable. Utilizing the eigenvalue decomposition, the symmetric Reynolds stress tensor $R_{ij} = \langle u_i u_j \rangle$ can be expressed as

$$R_{ij} = 2k\left(\frac{\delta_{ij}}{3} + v_{in}\Lambda_{nl}v_{lj}\right), \tag{1}$$

where k denotes the turbulent kinetic energy, v represents the eigenvector matrix, and Λ is the diagonal matrix of eigenvalues of the Reynolds stress tensor. The tensors v and Λ are ordered such that $\lambda_1 \geqslant \lambda_2 \geqslant \lambda_3$. The amplitude, the shape, and the orientation of the Reynolds stress are explicitly represented by k, λ_i, and v_{ij}, respectively. The objective of this study is to determine the possible range of Reynolds stresses, given a set of modeling assumptions. We specifically introduce a formal

strategy to perturb the eigenvalues and eigenvectors in Eq. (1) that does not rely on empirical data. Although it is also possible to design perturbations to the turbulent kinetic energy, no such attempt will be included here, in order to keep the current investigation free of user-specified parameters. The perturbations to the eigenvalues Λ are defined through the coordinates in the barycentric map $\mathbf{x}$ via $\lambda_i^* = B^{-1}\mathbf{x}^*$, where perturbed quantities are indicated by an asterisk and B is the transformation from the eigenvalue space to the barycentric triangle. The projection of the eigenvalue perturbation in the barycentric map has both a direction and a magnitude [4]. Considering the extreme states of Reynolds stress componentiality, we consider perturbation alignments to the three vertices of the triangle $\mathbf{x}_{1C}$, $\mathbf{x}_{2C}$, and $\mathbf{x}_{3C}$, representing the one-, two-, and three-component ($1C$, $2C$, and $3C$ hereafter) limiting states of turbulence anisotropy. The magnitude of the perturbation in the barycentric triangle is represented by $\Delta_B \in [0,1]$. Thus, the perturbed barycentric coordinates $\mathbf{x}^*$ are given by $\mathbf{x}^* = \mathbf{x} + \Delta_B(\mathbf{x}^{(t)} - \mathbf{x})$, where $\mathbf{x}^{(t)}$ denotes the target vertex (representing one of the $1C$, $2C$, or $3C$ limiting states) and $\mathbf{x}$ is the model prediction. Instead of relying on a user-defined Δ_B as in Ref. [4], we set $\Delta_B = 1$ so that the three limiting states are considered.

Virtually all RANS closures consider the turbulent kinetic energy evolution that satisfies the general form, directly derived from the Navier Stokes equations for an incompressible fluid

$$\frac{\partial k}{\partial t} + U_j \frac{\partial k}{\partial x_j} = -\frac{\partial T_i}{\partial x_i} + \mathcal{P} - \epsilon, \tag{2}$$

where $T_i = \frac{1}{2}\langle u_i u_j u_j\rangle + \langle u_i p\rangle/\rho - 2\nu\langle u_j s_{ij}\rangle$ represents the turbulent transport process, $\epsilon = 2\nu\langle s_{ij}s_{ij}\rangle$ is the dissipation rate, and $\mathcal{P} = -\langle u_i u_j\rangle \frac{\partial U_i}{\partial x_j}$ represents production. The production process represents the action of the mean velocity gradients working against the Reynolds stresses and represents a transfer of kinetic energy from the mean flow to the fluctuating velocity field. At the single-point description, this is the only turbulence process that is closed and does not require any simplifications or modeling, as opposed to, for instance, the pressure transport or the pressure strain correlation that are explicitly nonlocal. In this light, due to the inherent limitations imposed by the single-point nature of the classical modeling paradigm, production is the only turbulence process available to prescribe local eigenvector perturbations, without the need to introduce any additional modeling assumptions. Concordantly, the eigenvector perturbation methodology seeks to modulate the production mechanism. In the past, there have been attempts to extend the eigenspace perturbation framework to modulate the production mechanism. For instance, Gorlé *et al.* [6,14] have considered eigenvalue perturbations to the $1C$ and $3C$ limiting states of the componentiality and used the perturbed Reynolds stresses to calibrate the turbulent production. Similarly, Xiao *et al.* [15] have used a stochastic framework to formulate perturbations to the modeled Reynolds stress tensor. In this investigation, we focus on a purely physical approach, utilizing the dynamics of the production mechanism due to the eigenvector alignment of the Reynolds stresses. For the modulation of the production term, we consider the value of the Frobenius inner product $\langle A, R\rangle_F = \mathrm{tr}(AR)$, where A is the mean velocity gradient and R is the Reynolds stress. For the purpose of bounding this energy transfer, we seek the extremal states of production or the extremal values of the inner product. Based on works by Richter [16] and Lasserre [17], the sharpest bounds on $\langle A, R\rangle_F$ and their respective alignments can be derived. The corresponding bounds on the inner product are

$$\langle A, R\rangle_F \in [\lambda_1\gamma_3 + \lambda_2\gamma_2 + \lambda_3\gamma_1, \lambda_1\gamma_1 + \lambda_2\gamma_2 + \lambda_3\gamma_3], \tag{3}$$

where $\gamma_1 \geqslant \gamma_2 \geqslant \gamma_3$ are the eigenvalues of the symmetric component of A, explicitly, the mean rate of strain tensor. In the coordinate system defined by the eigenvectors of the rate of strain tensor, the alignments of the Reynolds stress eigenvectors for the bounding cases are given by $v_{\min} = \begin{bmatrix} 0 & 0 & 1 \\ 0 & 1 & 0 \\ 1 & 0 & 0 \end{bmatrix}$ and $v_{\max} = \begin{bmatrix} 1 & 0 & 0 \\ 0 & 1 & 0 \\ 0 & 0 & 1 \end{bmatrix}$.

To shed light onto this eigenspace perturbation framework, we outline a representative case schematically in Fig. 1. In Figs. 1(a1)–1(c1) we represent the Reynolds stress tensor at a specific

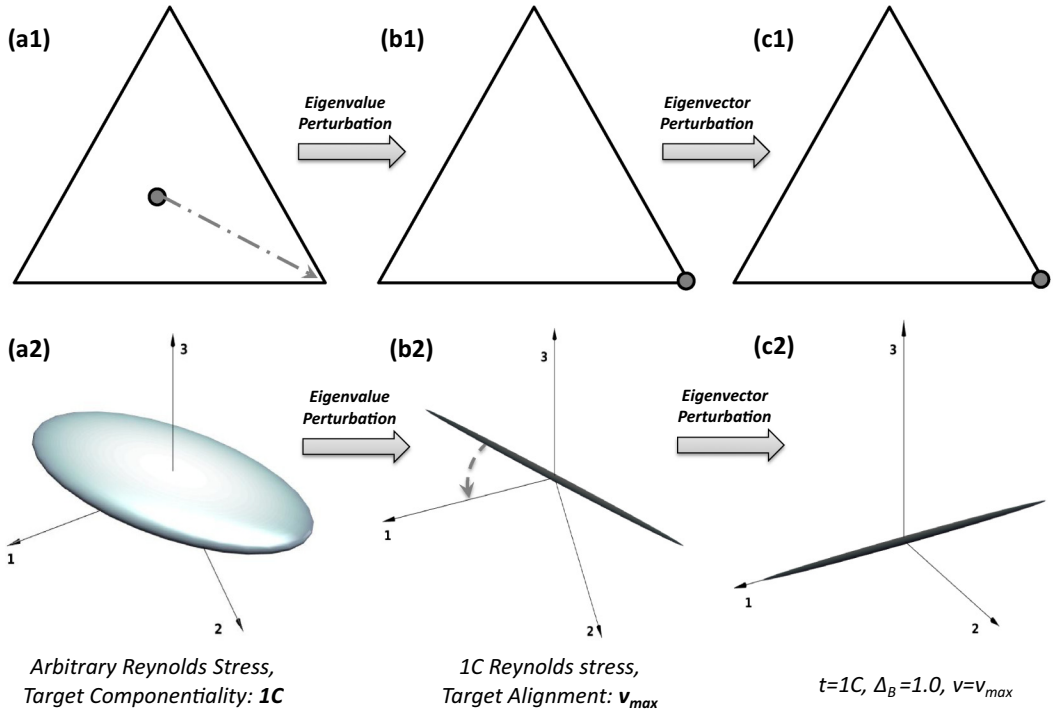

FIG. 1. Schematic outline of eigenspace perturbations from an arbitrary state of the Reynolds stress.

physical location in barycentric coordinates and in Figs. 1(a2)–1(c2) we visualize the Reynolds stress ellipsoid in a coordinate system defined by the mean rate of strain eigenvectors. These are arranged so that $\lambda_1 \geqslant \lambda_2 \geqslant \lambda_3$, so essentially the 1-axis is the stretching eigendirection and the 3-axis is the compressive eigendirection of the mean gradient.

Initially, the Reynolds stress predicted by an arbitrary model is exhibited in Figs. 1(a1) and 1(a2). The eigenvalue perturbation methodology seeks to sample from the extremal states of the possible Reynolds stress componentiality. Thus, we may, for instance, translate the Reynolds stress from a general three-component state to the $1C$ state, exhibited in the transition from Figs. 1(a1) to 1(b1). This translation changes the shape of the Reynolds stress ellipsoid from a a triaxial ellipsoid to an extreme prolate ellipsoid, exhibited in the transition from Figs. 1(a2) to 1(b2).

Thence, the eigenvector perturbation seeks to sample from the extremal states of the production mechanism, by varying the alignment of this ellipsoid. Thus, we may, for instance, rotate the Reynolds stress ellipsoid so that its semimajor axis is aligned with the stretching eigendirection of the mean rate of strain tensor, exhibited in the transition from Figs. 1(b2) to 1(c2). This particular alignment would enable us to analyze the impact of the maximum possible production on flow evolution. In conjunction, these two perturbation approaches enable us to maximize the information we may get from single-point statistics to quantify uncertainty bounds.

This eigenspace perturbation framework gives us five distinct extremal states of the Reynolds stress tensor; these are schematically displayed in Fig. 2. These correspond to three extremal states of the componentiality $(1C, 2C, 3C)$ and two extremal alignments of the Reynolds stress eigenvectors $(v_{\min}, v_{\max})$. For the $3C$ limiting state, the Reynolds stress ellipsoid is perfectly spherical. Due to its rotational symmetry at this state, all alignments of the spherical Reynolds stress ellipsoid are identical. Thus, for characterization of the eigenspace perturbation range on flow evolution, we need a set of only five RANS simulations.

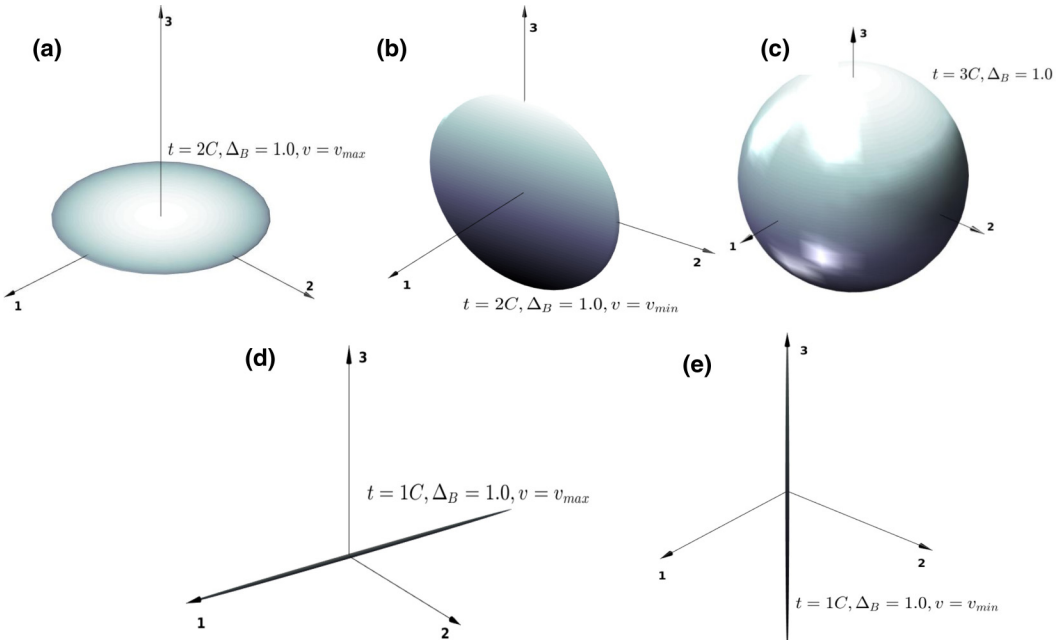

FIG. 2. Schematic visualization of the extremal states, as Reynolds stress ellipsoids, in the eigenspace perturbation methodology.

This methodology can be applied to any RANS-based model, including second moment closures. For the purposes of this investigation, we restrict ourselves to the shear stress transport (SST) model of Menter [18]. This explicitly means that the transport terms and the dissipation rate in Eq. (2) are obtained according to a simple eddy-viscosity closure. The results presented herein must be interpreted as the range of possible flow evolutions corresponding to the Reynolds stress eigenspace perturbations that are constrained by the SST model. Results corresponding to the SST model bereft of any perturbations are referred to as baseline solutions. A validated code using a structured finite-volume discretization, nominally second-order accurate spatially, was used for the simulations. In the next section, we apply this framework to canonical cases of separated turbulent flow in a planar diffuser and flow over a backward-facing step, along with a high-speed nozzle jet, detailed in Fig. 3. In these comparisons, eigenvalue perturbation refer to the approach wherein only the eigenvalues of the modeled Reynolds stress tensor are perturbed and the turbulence processes such as production are unchanged. Eigenspace perturbations refer to the approach wherein both eigenvalues and eigenvectors are perturbed as outlined in this section. As discussed, the eigenvector perturbations lead to a modulation of the turbulent production process.

III. RESULTS AND ANALYSIS

In the turbulent flow over a backward-facing step, the sudden domain expansion and the concomitant flow separation at the step generates a large recirculating region with high degrees of turbulent kinetic energy and significant negative velocity. In Fig. 4 the uncertainty bounds for the streamwise velocity profile at $x/H = 9$ are presented. At most of the points in the profile inside and beyond the separation zone, the eigenspace perturbation bounds are able to account for the discrepancy between model predictions and direct numerical simulation (DNS) data near the wall. Away from the wall, where the model prediction and the DNS data are in agreement, the uncertainty bounds are accordingly negligible. As can be seen, the uncertainty ranges induced by the eigenvalue perturbations alone are deficient and do not capture the true level of discrepancy.

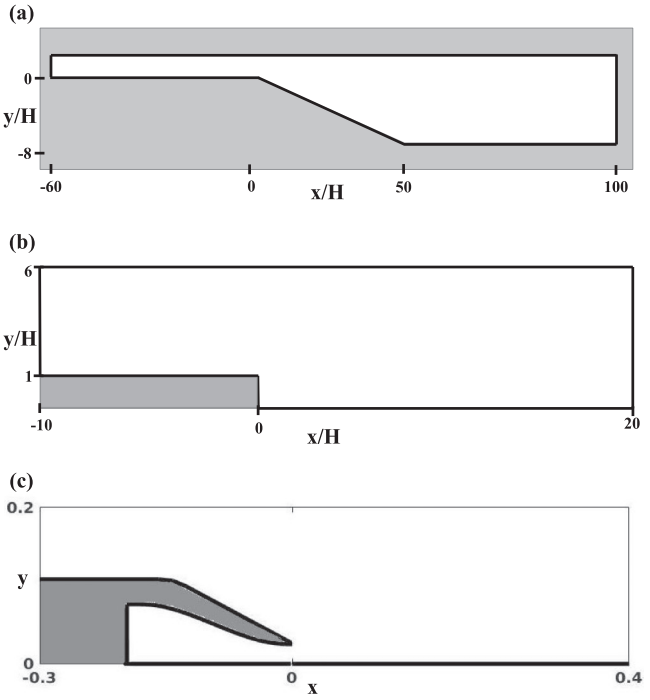

FIG. 3. Schematic detailing the flow cases investigated: (a) asymmetric diffuser, (b) backward-facing step, and (c) inset view of the ANR nozzle.

In Fig. 5 we consider the distribution of the skin-friction coefficient along the bottom wall. As can be observed, the uncertainty estimates from eigenspace perturbations are able to account for the discrepancy between model predictions and DNS data at most locations. The uncertainty bounds due to the eigenvalue perturbations are not able to address a significant proportion of the model inadequacy and essentially do not subsume the DNS data at any location. Figure 6 exhibits the flow streamlines in the zone of separation for this case. Variation in the alignment between the eigenvectors of the mean velocity gradient and the Reynolds stress modulates the production mechanism and

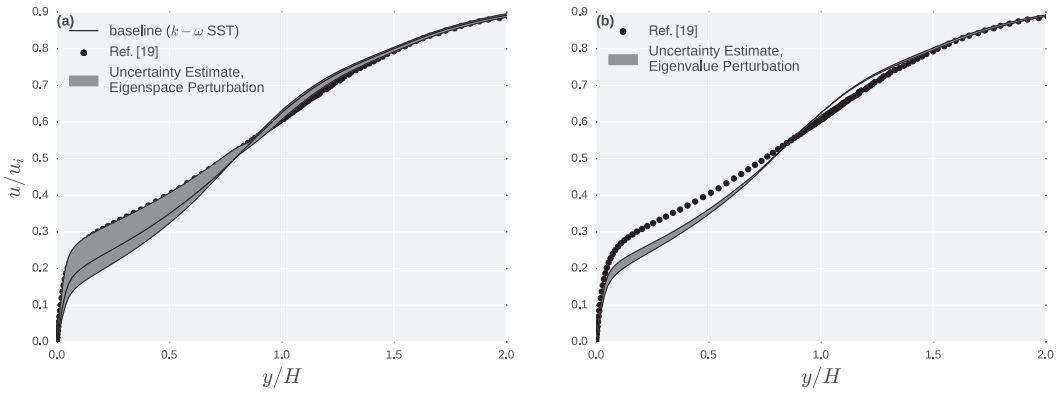

FIG. 4. Uncertainty estimates on the mean velocity profiles at $x/H = 9$: (a) eigenspace perturbation and (b) eigenvalue perturbation.

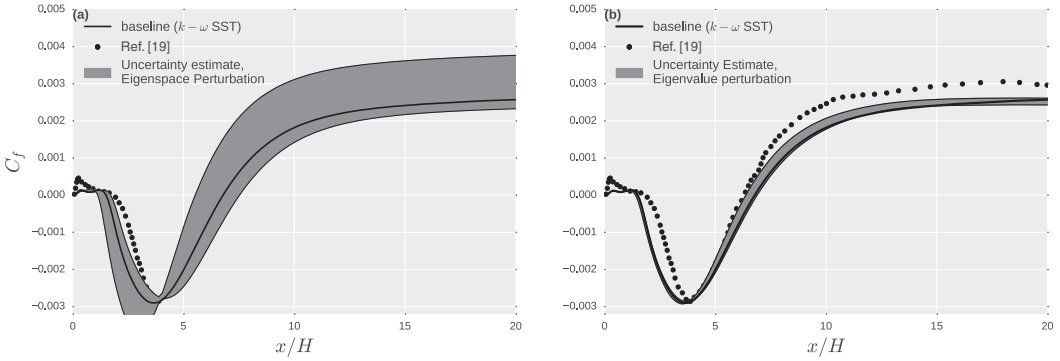

FIG. 5. Uncertainty estimates on the skin friction coefficient, contrasted against the DNS results of [19]: (a) eigenspace perturbation and (b) eigenvalue perturbation.

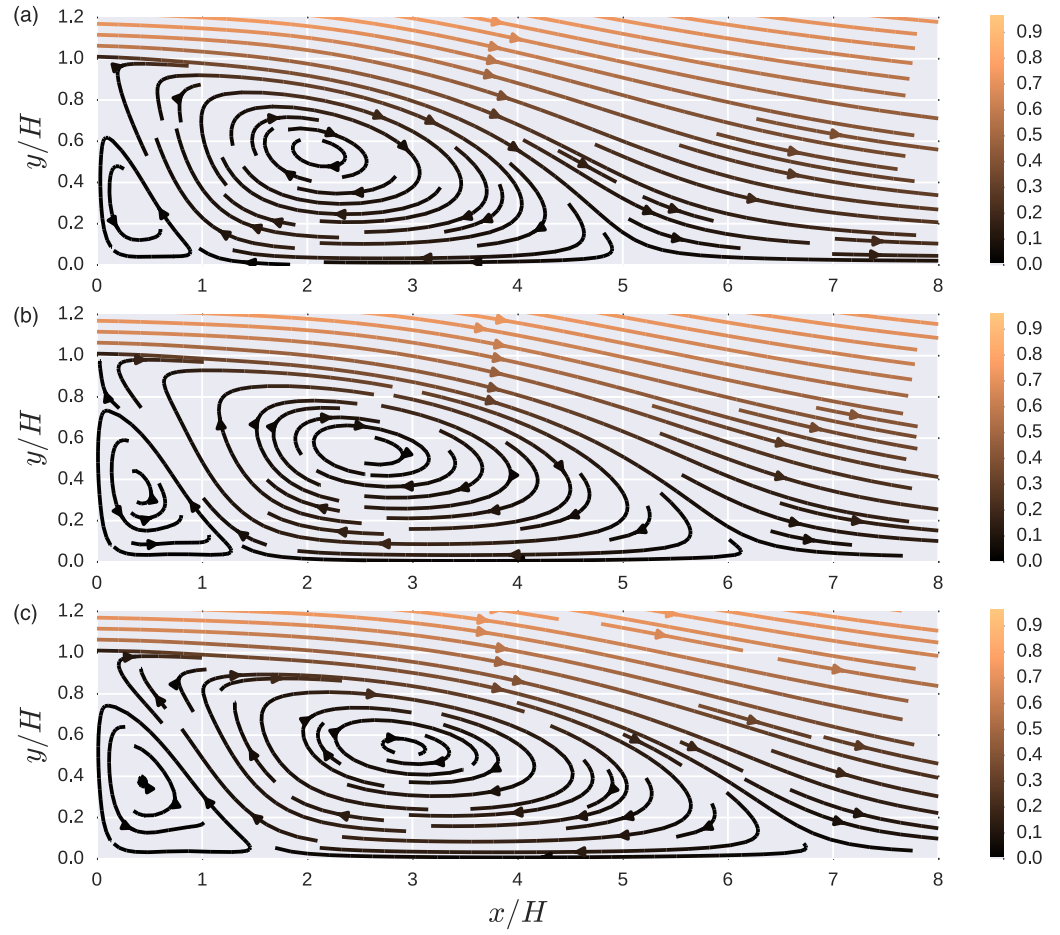

FIG. 6. Flow streamlines across the backward-facing step: (a) ($t = 1C, \Delta = 1.0, v = v_{\max}$), (b) baseline case, and (c) ($t = 3C, \Delta = 1.0, v = v_{\min}$).

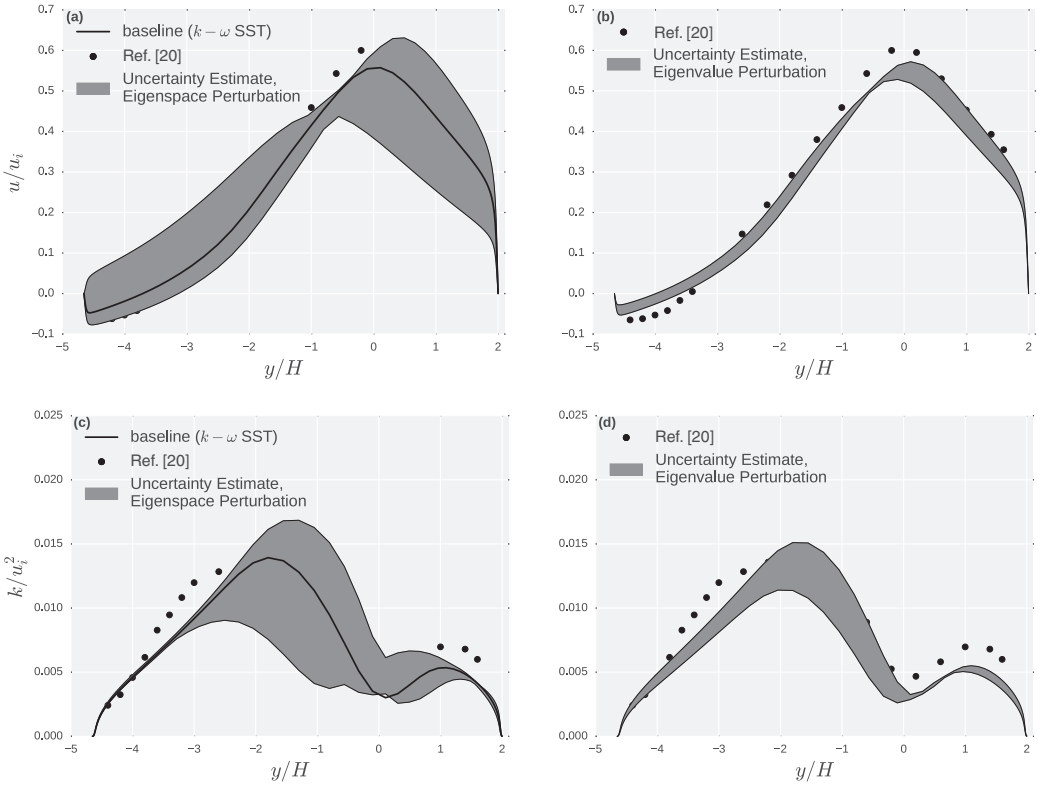

FIG. 7. Uncertainty estimates on the velocity and turbulent kinetic energy profiles at $x/H = 32$: (a) mean velocity, eigenspace perturbation; (b) mean velocity, eigenvalue perturbation; (c) turbulent kinetic energy, eigenspace perturbation; and (d) turbulent kinetic energy, eigenvalue perturbation.

results in significant changes in the resultant flow, as outlined in Figs. 6(a)–6(c). Bolstering the production process, for instance, via a perturbation represented mathematically as ($t = 1C, \Delta = 1.0$, $v = v_{\max}$) reduces the flow separation [Fig. 6(a)] as compared to the baseline flow [Fig. 6(b)]. Contrarily, damping production, for instance, using a perturbation classified by ($t = 3C, \Delta = 1.0$, $v = v_{\min}$) leads to the opposite effect and leads to a larger zone of separated flow [Fig. 6(c)].

The turbulent flow in a plane diffuser involves separation from a smooth wall due to an adverse pressure gradient and subsequent reattachment, followed by redevelopment of the boundary layer in the downstream. Each of these features offers challenges for RANS models. In Fig. 7 we outline the uncertainty bounds for the mean velocity and the turbulent kinetic energy at $x/H = 32$. As can be seen, for the mean velocity, the eigenspace perturbation framework is able to provide uncertainty bounds that encompass the experimental data at most locations along the profile. The results of the eigenvalue perturbation methodology are again limited in accounting for the discrepancy between the model predictions and the experimental data. Similar results may be inferred for the turbulent kinetic energy profiles.

In Fig. 8 the bounds on the skin-friction coefficient are considered. As can be seen, the eigenspace perturbations engender bounds that account for a significant proportion of the discrepancy between RANS predictions and experimental data. On contrasting the results of the eigenspace perturbation framework against the eigenvalue-only perturbations, it is evident that the latter are considerably more limited in capturing the discrepancy. Figure 9 exhibits the flow streamlines across the diffuser for the two cases wherein the production mechanism is bolstered [Fig. 9(a)] and damped [Fig. 9(c)] via the alignment of the eigenvectors of the perturbed Reynolds stresses, contrasted against the

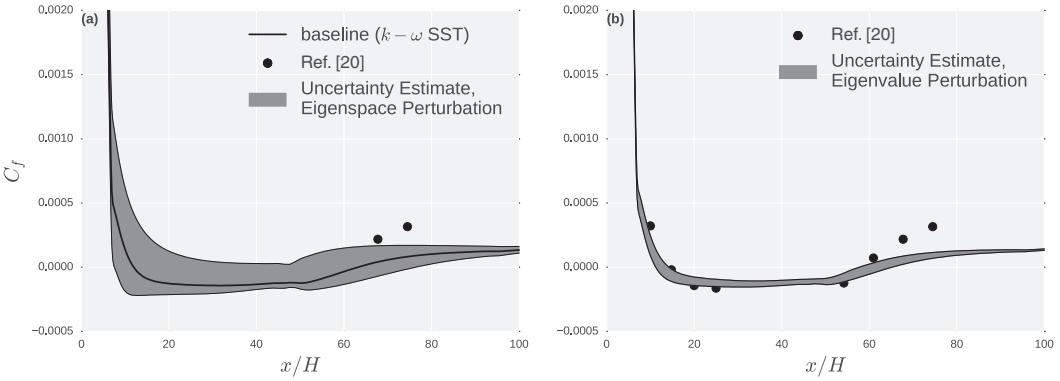

FIG. 8. Uncertainty estimates on the skin friction coefficient, contrasted against the experimental results of [20]: (a) eigenspace perturbation and (b) eigenvalue perturbation.

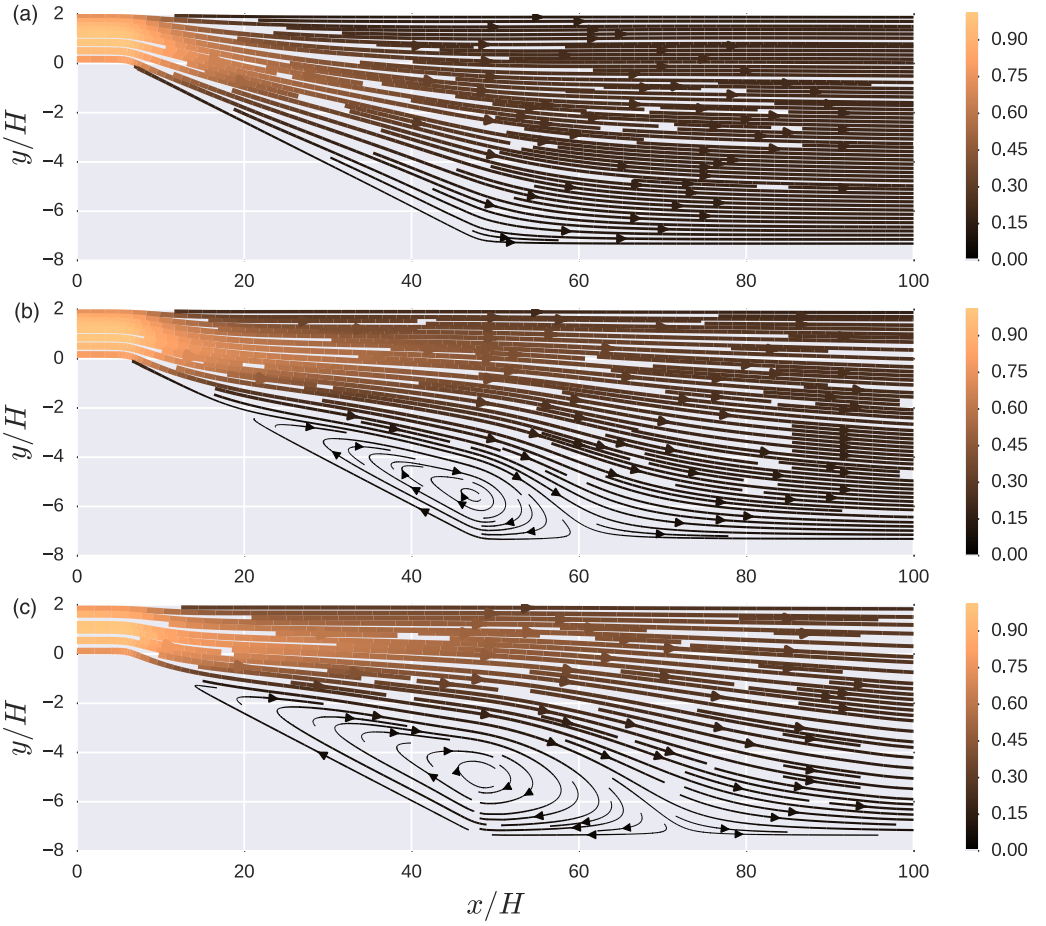

FIG. 9. Flow streamlines across the diffuser geometry: (a) ($t = 1C, \Delta = 1.0, v = v_{\max}$), (b) baseline case, and (c) ($t = 3C, \Delta = 1.0, v = v_{\min}$). The contour shading represents the magnitude of the streamwise velocity, while the streamline thicknesses are scaled with the magnitude of the total mean velocity.

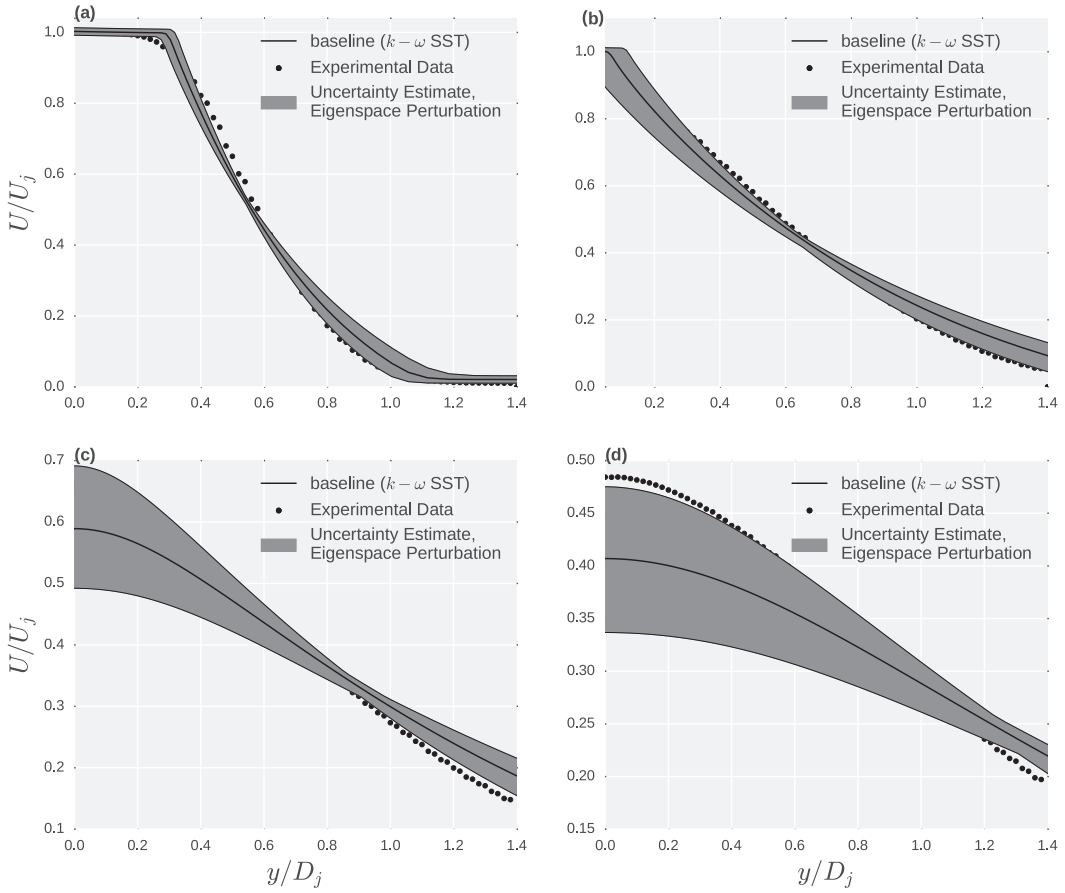

FIG. 10. Uncertainty estimates on the axial velocity profiles, contrasted against experimental results of [22]: (a) $x/D_j = 4$, (b) $x/D_j = 8$, (c) $x/D_j = 12$, and (d) $x/D_j = 16$.

baseline predictions of the SST model [Fig. 9(c)]. As was exhibited for the backward-facing step, bolstering the production process suppresses the flow separation, while damping the production mechanism leads to a broader zone of separated flow.

The third flow case deals with the high-speed turbulent jet from an aircraft nozzle. While RANS models are applied routinely in the simulation of turbulent jet flow fields issuing from aircraft engine exhaust nozzles, they have many limitations. For instance, most models predict a significantly lower rate of initial jet mixing as contrasted against high-fidelity data [21]. Furthermore, farther downstream of the jet potential core, RANS models predict the far-field mixing rate to become higher than is seen in experimental data [22]. Figure 10 outlines the uncertainty estimates for the axial velocity profiles for a turbulent jet from an aircraft nozzle. The velocity profiles for the upper half of the nozzle are outlined up to 1.4 nozzle diameters for which experimental data were available. The lengths and velocities are scaled by the nozzle exit diameter D_j and the jet exit velocity U_j. The experimental data [22] correspond to a cold Mach 0.52 jet effluxing from a convergent nozzle (specifically, the NASA Acoustic Response Nozzle design) into a quiescent ambient. As is exhibited in the figures, the uncertainty estimates from the eigenspace perturbations are able to account for a significant proportion of the discrepancy between the particle-image velocimetry data and the RANS model predictions, both in the initial development region and far downstream of the nozzle exit.

From the results presented herein, it is evident that the proposed eigenspace perturbations lead to uncertainty ranges that can account for a significant proportion of the observed model discrepancy.

In the flow cases considered, this framework is able to exhibit uncertainty ranges that provide a judicious lower bound on the uncertainty in predictions and thus may even be of utility in the engineering design process. In some situations the experimental measurements (or the corresponding high-fidelity simulation data) remain beyond the predicted ranges. One possible explanation is the inherent limitation of the present perturbation framework, as it does not include a spatial dependence of the perturbations and an explicit characterization of the errors induced by the modeling of the turbulent transport and the dissipation rate in Eq. (2). However, it is important to outline that in some cases, the differences are due to other assumptions in the computations, such as the use of steady two-dimensional simulations to represent a potentially unsteady three-dimensional flow, such as the flow reattachment in the asymmetric diffuser [23].

IV. CONCLUSION AND FUTURE WORK

In this investigation, we outlined a framework for estimating structural uncertainty bounds on RANS-based closures. This methodology incorporates both eigenvalue and eigenvector perturbations in the spectral representation of the Reynolds stress tensor. To ensure the engineering applicability of this framework, we constrained ourselves to single-point statistics and locally closed turbulence processes. In this regard, the eigenvector perturbations are guided by the modulation of the production process. Using an analytical approach, the sharpest bounds on the production process and the Reynolds stress eigenvector alignments corresponding to the same were derived. This framework was applied to a set of turbulent flows with separation, while contrasted against numerical and experimental data and compared to the bounds due to an eigenvalue-only perturbation methodology. It was exhibited that for all cases, this procedure is able to provide prudent estimates on the uncertainty of quantities of interest.

Without a reliable procedure to account for the uncertainty induced by the modeling of the turbulent transport and dissipation rate in the turbulent kinetic energy evolution equations, there remain facets of model uncertainty that we did not account for. Similarly, the absence of a theoretical framework to describe the spatial discrepancy limited the comprehensive nature of the analysis. However, using these comparisons, we have attempted to exhibit that for separated flows, the eigenspace perturbation framework is able to provide considerable improvement over the extant eigenvalue perturbation methodology, without introducing further assumptions or correlations to empirical data. Additionally, the uncertainty bounds engendered herein are relatively easy to compute and may be of potential engineering utility to guide design decisions.

In general incompressible turbulent flows, the key physical mechanism driving turbulence is the production process. Thus, we utilized this single-point phenomenon to identify extremal states for the estimated bounds. In other applications, for instance, buoyancy-driven turbulent flows, additional physical mechanisms will be present and either theoretical or numerical investigations may be used to identify the extremal states, leading to the estimation of requisite uncertainty bounds. Further work in this direction may be of great engineering interest.

ACKNOWLEDGMENT

This research was supported by the Defense Advanced Research Projects Agency under the Enabling Quantification of Uncertainty in Physical Systems project.

[1] A. P. Singh and K. Duraisamy, Using field inversion to quantify functional errors in turbulence closures, Phys. Fluids **28**, 045110 (2016).

[2] E. J. Parish and K. Duraisamy, A paradigm for data-driven predictive modeling using field inversion and machine learning, J. Comput. Phys. **305**, 758 (2016).

[3] J. Ling and J. Templeton, Evaluation of machine learning algorithms for prediction of regions of high Reynolds averaged Navier Stokes uncertainty, Phys. Fluids **27**, 085103 (2015).
[4] M. Emory, J. Larsson, and G. Iaccarino, Modeling of structural uncertainties in Reynolds-averaged Navier-Stokes closures, Phys. Fluids **25**, 110822 (2013).
[5] C. Gorlé and G. Iaccarino, A framework for epistemic uncertainty quantification of turbulent scalar flux models for Reynolds-averaged Navier-Stokes simulations, Phys. Fluids **25**, 055105 (2013).
[6] C. Gorlé, C. Garcia-Sanchez, and G. Iaccarino, Quantifying inflow and RANS turbulence model form uncertainties for wind engineering flows, J. Wind Eng. Ind. Aerodyn. **144**, 202 (2015).
[7] A. A. Mishra, G. Iaccarino, and K. Duraisamy, Epistemic uncertainty in statistical Markovian turbulence models, Annual Research Briefs (Center for Turbulence Research, Stanford University, 2015), pp. 183–195.
[8] A. A. Mishra and G. Iaccarino, RANS predictions for high-speed flows using enveloping models, Annual Research Briefs (Center for Turbulence Research, Stanford University, 2016), pp. 289–301.
[9] H. Xiao, J.-L. Wu, R. Wang, and C. J. Roy, Quantifying and reducing model form uncertainties in Reynolds-averaged Navier-Stokes simulations: A data-driven, physics-informed approach, J. Comput. Phys. **324**, 115 (2016).
[10] J.-L. Wu, J.-X. Wang, and H. Xiao, A Bayesian calibration-prediction method for reducing model-form uncertainties with application in RANS simulations, Flow Turbul. Combust. **97**, 761 (2016).
[11] C. G. Speziale, T. B. Gatski, and N. M. G. Mhuiris, A critical comparison of turbulence models for homogeneous shear flows in a rotating frame, Phys. Fluids **2**, 1678 (1990).
[12] A. A. Mishra and S. S. Girimaji, On the realizability of pressure-strain closures, J. Fluid Mech. **755**, 535 (2014).
[13] B. E. Launder, D. P. Tselepidakis, and B. A. Younis, A second-moment closure study of rotating channel flow, J. Fluid Mech. **183**, 63 (1987).
[14] C. Gorlé, M. Emory, J. Larson, and G. Iaccarino, *Epistemic Uncertainty Quantification for RANS Modeling of the Flow over a Wavy Wall*, Center for Turbulence Research Annual Research Briefs (Stanford University Press, Stanford, 2012), pp. 81–91.
[15] H. Xiao, J.-X. Wang, and R. G. Ghanem, A random matrix approach for quantifying model-form uncertainties in turbulence modeling, Comput. Meth. Appl. Mech. Eng. **313**, 941 (2017).
[16] H. Richter, Zur abschätzung von matrizennormen, Math. Nachr. **18**, 178 (1958).
[17] J. B. Lasserre, A trace inequality for matrix product, IEEE Trans. Automatic Control **40**, 1500 (1995).
[18] F. R. Menter, Two-equation eddy-viscosity turbulence models for engineering applications, AIAA J. **32**, 1598 (1994).
[19] H. Le, P. Moin, and J. Kim, Direct numerical simulation of turbulent flow over a backward-facing step, J. Fluid Mech. **330**, 349 (1997).
[20] C. U. Buice and J. K. Eaton, Experimental investigation of flow through an asymmetric plane diffuser, Annual Research Briefs (Center for Turbulence Research, Stanford University, 1996), p. 243.
[21] N. J. Georgiadis, D. A. Yoder, and W. B. Engblom, Evaluation of Modified Two-Equation Turbulence Models for Jet Flow Predictions, AIAA J. **44**, 3107 (2006).
[22] J. Bridges and M. P. Wernet, The NASA Subsonic Jet Particle Image Velocimetry (PIV) Dataset, NASA TM 2011-216807, Nov. 2011.
[23] H.-J. Kaltenbach, M. Fatica, R. Mittal, T. S. Lund, and P. Moin, Study of flow in a planar asymmetric diffuser using large-eddy simulation, J. Fluid Mech. **390**, 151 (1999).